Coherent-Phonon-Driven Intervalley Scattering and Rabi Oscillation in Multivalley 2D Materials

Chenyu Wang,[1,2,*] Xinbao Liu,[1,2,*] Qing Chen,[1,2,*] Daqiang Chen,[1] Yaxian Wang [1,†] and Sheng Meng [1,2,3,‡]

[1]*Beijing National Laboratory for Condensed Matter Physics and Institute of Physics,*
Chinese Academy of Sciences, Beijing 100190, China
[2]*School of Physical Sciences, University of Chinese Academy of Sciences, Beijing 100190, China*
[3]*Songshan Lake Materials Laboratory, Dongguan, Guangdong 523808, China*

Resolving the complete electron scattering dynamics mediated by coherent phonons is crucial for understanding electron-phonon couplings beyond equilibrium. Here we present a time-resolved theoretical investigation on strongly coupled ultrafast electron and phonon dynamics in monolayer WSe$_2$, with a focus on the intervalley scattering from the optically "bright" K state to "dark" Q state. We find that the strong coherent lattice vibration along the longitudinal acoustic phonon mode [$LA(M)$] can drastically promote K-to-Q transition on a timescale of ∼400 fs, comparable with previous experimental observation on thermal-phonon-mediated electron dynamics. Further, this coherent-phonon-driven intervalley scattering occurs in an unconventional *steplike* manner and further induces an electronic Rabi oscillation. By constructing a two-level model and quantitatively comparing with *ab initio* dynamic simulations, we uncover the critical role of nonadiabatic coupling effects. Finally, a new strategy is proposed to effectively tune the intervalley scattering rates by varying the coherent phonon amplitude, which could be realized via light-induced nonlinear phononics that we hope will spark experimental investigation.

Monolayer transition metal dichalcogenides (TMDCs) have captured extensive attention in the scientific community in the past decades [1–5]. Alongside tremendous potential for innovative applications, their band structure that endows electrons with an extra valley degree of freedom further allows the study of fundamental many-body processes [3,5]. In particular, the intervalley scattering of free carriers or bounded excitons with lattice vibrations, namely phonons, has long been of central interest. As an important mechanism for valley depolarization that concerns the realization of practical valleytronics [3,6], a microscopic investigation of this process would be crucial for technological manipulation as well as for fundamental physical understanding.

Early works focus mainly on the intervalley scattering dynamics mediated by thermal phonons, where the electron-phonon coupling (EPC) is vital to determine the scattering rates and thus the electronic dynamics. Therein, although mode-resolved EPC strength could be obtained from *ab initio* calculations [7–11], available experiments are limited as they capture the dynamics for specific electronic states yet mediated by all phonon modes [12–15]. To resolve the contributions from the individual phonon mode, one has to excite it coherently, thereby driving the system out of equilibrium [16,17]. Recently, selective excitation of lattice vibration as coherent phonons has dramatically facilitated the dynamical control of materials' properties, such as switching lattice symmetry [18–21], engineering topological

properties [22–25], enhancing superconductivity [26,27], and manipulating carrier lifetimes [28–30]. In particular, theoretical and experimental investigations have recently emerged to detect band- and mode-selective EPC under such nonequilibrium conditions [31–35]. However, the complete microscopic dynamics of photoexcited electrons scattered by nonequilibrium coherent phonons in monolayer TMDCs is unclear, and experimental insight into this process remains hard to achieve due to the difficulty in launching selected coherent phonon modes. Therefore, first-principle study in femtosecond time regime becomes urgently needed to calibrate and guide ultrafast intervalley scattering dynamics assisted by coherent phonons.

In this Letter, we study the coupled ultrafast electron and lattice dynamics after laser excitation within the formalism of real-time time-dependent density functional theory based molecular dynamics (TDDFT-MD) [36–39], focusing on coherent-phonon-driven intervalley scattering between the K and Q valleys in monolayer WSe$_2$, a prototypical semiconductor in the TMDC family. By evolving electron occupation with the presence of coherent oscillation of a longitudinal acoustic phonon mode at M point in the Brillouin zone, LA(M), we observe a *steplike* transition of the resonantly pumped K valley electrons to the Q valley. Further, the K-to-Q transition driven by coherent phonons with large amplitude occurs on a timescale of ∼400 fs, comparable with previous experimental observations under thermal phonon conditions [12].
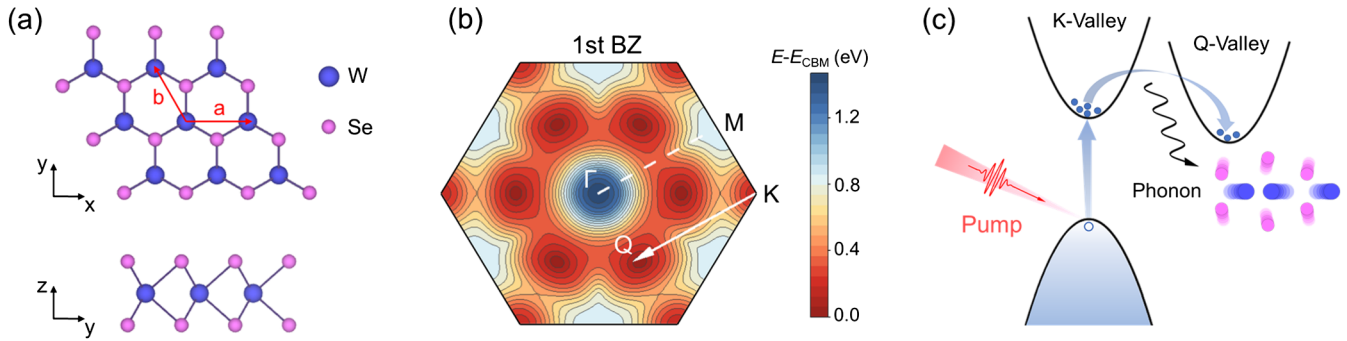
FIG. 1. (a) Top and side view of the monolayer WSe_2 lattice. (b) Contour plot of the lowest energy conduction band in the first Brillouin zone (black line) showing the K and Q valley as local minima. (c) Schematic illustration of phonon-mediated intervalley scattering upon photoexcitation. The momentum compensation is provided by the M point zone-boundary phonon [white arrow in (b)], depicted by the atomic displacements imposing on the pristine lattice.

We construct a two-level Hamiltonian and extrapolate the time-dependent nonadiabatic coupling matrix element (NACME), which is strongly coupled to the steplike intervalley scattering. Furthermore, we show that this K-to-Q scattering process is highly tunable by either directly varying the phonon amplitude, or by indirect manipulation via nonlinear phononics. Finally, we uncover a reversible dynamics of electrons scattering back to the K valley on a longer timescale, analogous to "Rabi oscillation" but induced by the nonequilibrium coherent phonons, which may invoke brand-new applications in valleytronics.

Ultrafast electron-lattice dynamics.—Monolayer WSe_2 has a sandwiched composition of Se-W-Se where the metal and chalcogen atoms are arranged periodically forming a hexagonal lattice [see Fig. 1(a) for the top and side view]. Its electronic structure features an indirect band gap with the valence and conduction band extrema at the K and Q point, respectively. There is also a sublowest unoccupied K valley with a tiny energy difference of 60 meV, shown in the energy contour plot in Fig. 1(b).

Under photoexcitation resonant with the direct gap at K valley (1.74 eV), only the optically "bright" state forms, and its subsequent relaxation to the "dark" Q state could be realized with the assistance of short-wavelength phonons with certain momentum compensation, specifically, the $LA(M)$ mode with its wave vector denoted by the dashed line in Fig. 1(b). Such a process is schematically illustrated in Fig. 1(c).

To study such ultrafast electron dynamics after photoexcitation, we start from a 2×2 supercell displaced along the eigenvector of the $LA(M)$ mode with an amplitude of ~ 1.7 Å$\sqrt{amu}$ and then resonantly excite the K valley electrons with a Gaussian enveloped laser pulse (Supplemental Material [40], Fig. S1). The middle panel of Fig. 2(c) shows the coherent lattice motion with frequency of 3.09 THz, consistent with the $LA(M)$ mode yet has been largely softened due to excited carriers (Table I in Sec. S6 in the Supplemental Material [40]).

We also track the evolution of the electronic system in its excited state, showing the transient band structure at 160 and 240 fs in Fig. 2(b). The red (blue) colored subbands containing the K (Q) valley, which have been folded to the same point in the reduced Brillouin zone [Fig. 2(a)], undergo a dramatic change along with lattice vibrations. For the time evolution of the K/Q valleys, we again observe a simultaneous oscillation of their instant eigenvalues, shown in the upper panel of Fig. 2(c). Intriguingly, the electronic system exhibits half of the period of the lattice dynamics [Figs. 2(a) and 2(b)], arising from the translational equivalence of the transient crystal structures separated by half of the phonon period (Sec. S7 in the Supplemental Material [40]).

Furthermore, we investigate the population dynamics of photocarriers at the two valleys by calculating their occupation number, and simulating the momentum-resolved photoemission signal. Figure 2(d) shows different snapshots following an external laser pulse. Initially ($t = 40$ fs), only the "bright" K valley undergoes a rapid electron population, as expected for resonant excitation. The signal diminishes at later times while the "dark" Q valley population clearly builds up at $t \sim 300$ fs, until the Q valley states dominate the emission signal at $t \sim 500$ fs. To our best knowledge, such coherent-phonon-driven phenomena have not been demonstrated yet, as most time-resolved measurements are performed at finite temperature with thermal phonons dominating. Nevertheless, by calculating the ratio of the K/Q population, we find a comparable timescale of electron transition in comparison with previous experimental observation, yet achieved by coherent lattice excitation; see Fig. 2(d). We attribute this similar timescale in both coherent and thermal phonon conditions to the intrinsically strong coupling of the $LA(M)$ mode with the valley states.

However, the complete *coherent-phonon-driven* electronic dynamics exhibit a steplike behavior [Fig. 2(c), lower panel], which is the most distinguishable feature compared with the exponential decay under thermal equilibrium
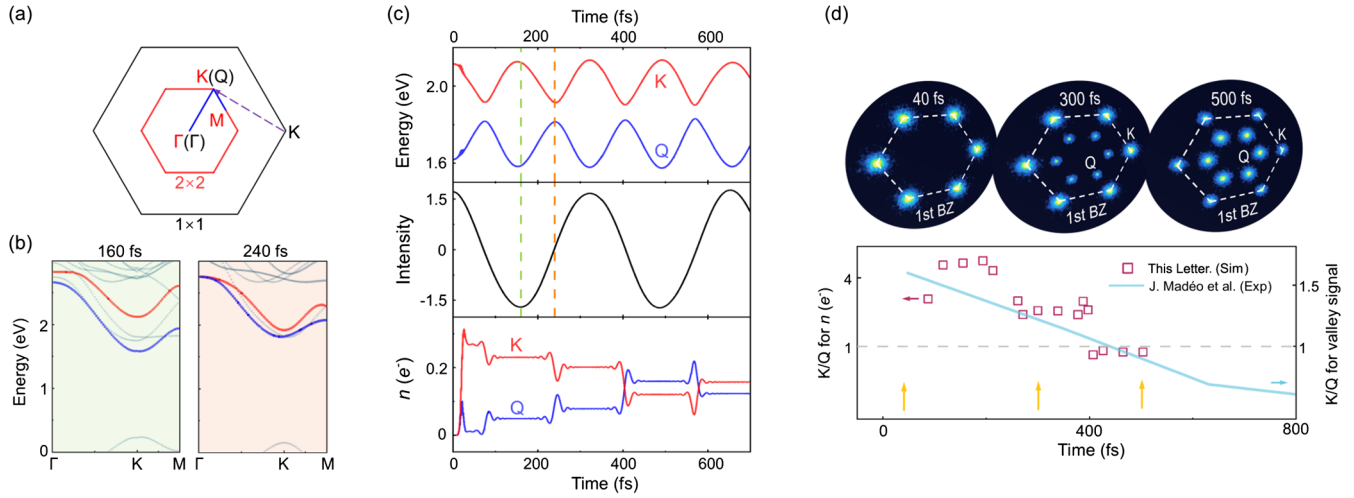
FIG. 2.   (a) Two-dimensional Brillouin zone of the hexagonal unit cell and the 2×2 supercell with their high symmetry points colored black and red, respectively. K and Q valleys share the same wave vector upon zone folding indicated by the purple dashed line. (b) Real-time band structure at 160 and 240 fs where the band containing the K (Q) valley is colored in red (blue). (c) Upper panel: time evolution of instantaneous eigenvalue of the K and Q valley. Middle panel: Atomic motion projected onto the eigenvector of the LA(M) mode. The colored dashed lines denote the snapshots chosen for band structures plotted in (b). Lower panel: electron occupation of the K and Q valley upon laser excitation imposed at $t = 20$ fs. (d) Momentum-resolved photoemission signal simulated at 40, 300, and 500 fs for a direct visualization of the K-to-Q intervalley scattering, with the K/Q ratio for the occupation number shown by red squares. At a timescale of ~400 fs, the occupation of the Q valley exceeds that of K (gray dashed line), comparable with a previous experimental study [12] shown by the blue line.

conditions (Sec. S3 in the Supplemental Material [40]). Here, we focus first on the K-to-Q transition within ~500 fs, and the subsequent reversed transition which we have referred to as "Rabi oscillation" will be discussed later (see the Supplemental Material [40] Fig. S4 for a full K-Q-K Rabi oscillation cycle). Remarkably, when comparing the middle and lower panels of Fig. 2(c), we again observe a strong correlation between the transient occupation number and the structural dynamics. Immediately one can see that electrons transfer from the K to Q valley when the atoms are moving close to their equilibrium positions with a maximum velocity, while negligible transition happens when the lattice is deformed to a large amplitude, i.e., a minimal atomic velocity, indicating the atomic motion may act as a trigger for such steplike transitions.

This is in contrast with the thermal (quasi-)equilibrium conditions, where thermal phonons are treated as static perturbations and the electronic dynamics show no dependence on the velocity of atomic motion [9,58]. Therefore, this steplike behavior coupling with the lattice dynamics is distinctive and likely due to the *far-from-equilibrium* conditions where electrons are optically excited and lattice vibrations are coherently driven.

We do note that the excitonic effect is not negligible in two-dimensional TMDCs, especially in optical responses. In the context of coherent-phonon-driven intervalley scattering, we estimated the exitonic effect by explicitly including the long-range electron-hole Coulomb interaction in our TDDFT calculations, and find no noticeable change in the scattering features (Sec. S4 of the

Supplemental Material [40]). This is in agreement with previous studies, where the electron-phonon coupling has the largest contribution (~7 meV) to the nonadiabatic coupling in phonon-induced bright-to-dark exciton dynamics, at least 1 order of magnitude larger than the electron-hole Coulomb interactions (~0.06 meV) [13,59]. Therefore, we conclude that the specific strong electron-phonon coupling with the LA(M) mode allows for a distinct coherent-phonon-driven scattering mechanism, which is robust and not subject to the long-range electron-hole interaction.

The nonadiabatic coupling matrix element.—To better understand the physical picture of the ultrafast electron dynamics, we construct a simplified two-level Hamiltonian as

$$\hat{H} = \begin{pmatrix} \varepsilon_K & \mathcal{D}d(t) \\ \mathcal{D}d(t) & \varepsilon_Q \end{pmatrix}, \qquad (1)$$

where ε_K, ε_Q are the static energies of the K and Q state, and $\mathcal{D}$ is defined as the deformation potential [60–62] that quantifies the electron-phonon coupling strength [41,63] (Sec. S9 of the Supplemental Material [40]). $d(t) = A\cos(\omega t)$ describes the atomic motion along the LA(M) mode, with A and ω being the normal mode amplitude and frequency. Using parameters listed in Table II in Sec. S9 of the Supplemental Material [40], we compute the instantaneous $K(Q)$ valley eigenvalues shown in Fig. 3(a). The TDDFT results are plotted again for a direct comparison,
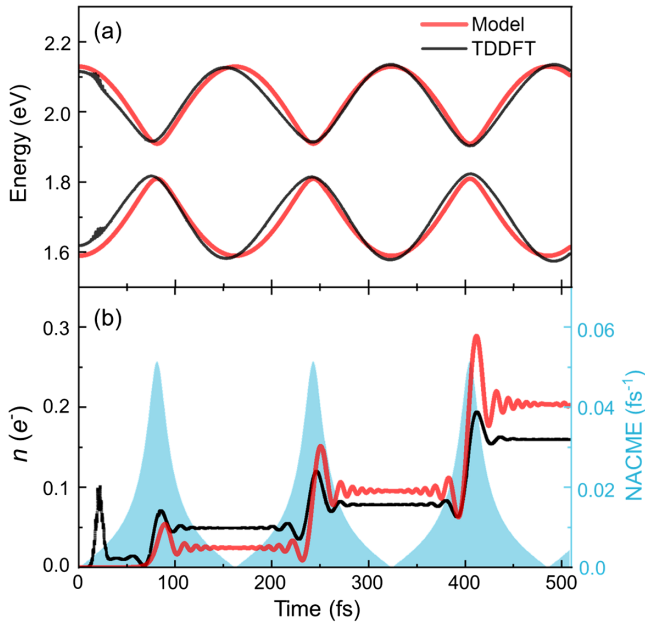
FIG. 3.   (a) The instantaneous eigenvalue and (b) the electron occupation of the Q valley calculated from the model Hamiltonian (red) and TDDFT simulations (black). The shaded area in (b) represents the NACME value.

where the excellent agreement validates our analytical model Hamiltonian.

To further elucidate the coupling of phononic and electronic degree of freedom, we provide a nonadiabatic perspective into the scattering dynamics [64,65] (Sec. S8 of the Supplemental Material [40]). On the grounds of that, we obtain the electron population on the Q valley as [42]

$$n_Q(t) = \left| \int_0^t dt_1 e^{-\frac{i}{\hbar}\int_{t_1}^t dt' \varepsilon_Q(t')} \langle \dot{Q}(t_1)|K(t_1)\rangle e^{-\frac{i}{\hbar}\int_0^{t_1} dt' \varepsilon_K(t')} \right|^2,$$

$$(2)$$

and the K valley occupation number is obtained by particle conservation. This allows us to extract the NACME

$\langle \dot{Q}(t)|K(t)\rangle$ that describes the breakdown of the adiabatic approximation,

$$\langle \dot{Q}(t)|K(t)\rangle = \frac{\mathcal{D}\dot{d}(t)}{\varepsilon_Q(t) - \varepsilon_K(t)}.$$

$$(3)$$

As shown in Fig. 3(b), our two-level Hamiltonian successfully reproduces the steplike behavior. Interestingly, we find the scattering dynamics is mostly governed by the NACME, that is, the steplike transition between the K and Q valley occurs where the NACME exhibits a sharp peak, whereas small NACME leaves the electron population on the two valleys oscillating about their stable values. Again, we see a correspondence of NACME with the atomic velocity, accompanied by a narrowed gap between the K and Q state [Eq. (3)]. Therefore, such strong a coherent perturbation breaks down the adiabatic limit, and the nonadiabatic electron-phonon coupling effect instead is responsible for the steplike scattering dynamics.

Manipulating K-to-Q scattering by coherent phonons.— We perform TDDFT calculations with two other optical phonon modes but find negligible K-to-Q scattering. This is closely related to the *mode-selective* electron-phonon coupling strength, or more precisely, the deformation potential and its effect on the NACME [Fig. S7(b) in the Supplemental Material [40]]. More importantly, we find the NACME can be largely enhanced by the coherent phonon amplitude (Fig. S7(c)), offering an alternative avenue toward engineering the intervalley scattering in TMDCs that is hard to achieve under equilibrium conditions.

To validate this effect, we perform further TDDFT calculations to simulate the evolution of K and Q valley occupation with different LA(M) phonon amplitudes. We define the transition rate as the normalized amount of electrons transferred from the K to Q valley during the half Rabi oscillation cycle, and its dependence on the LA(M) phonon amplitude is shown in Fig. 4(a). About 40% more electrons are scattered from the K to Q valley when the phonon amplitude increases from 0.6 to 1.7 Å$\sqrt{\text{amu}}$,
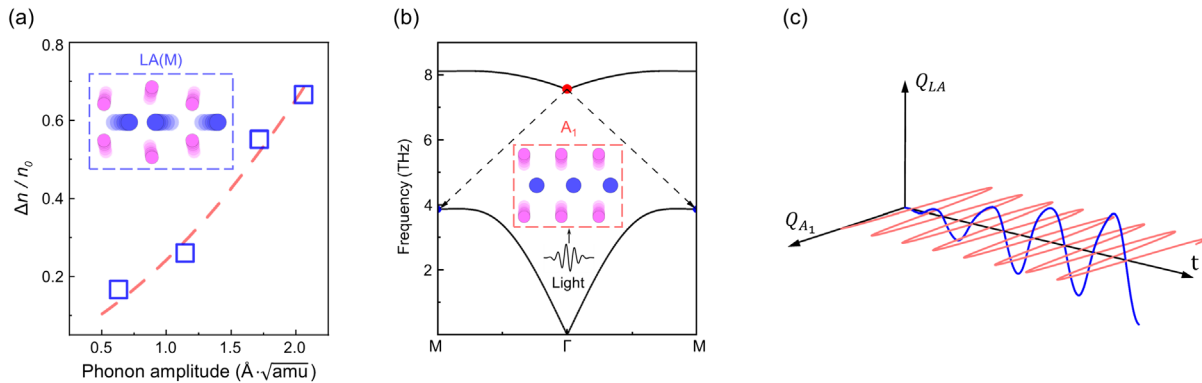

FIG. 4.   (a) Modulation of electron transition rate by varying phonon amplitude. Red dashed line is a polynomial fit to guide the eye. (b) Down-conversion decay channel of A_1 phonon into a pair of LA phonons at M. (c) Phonon amplitude of LA(M) and A_1 modes within a MD simulation period of 1 ps.

tantamount to a few percent of Angstrom for each atom. Therefore, apart from the electron-phonon coupling strength, we propose the phonon amplitude to be a unique medium for effective manipulation of valley depolarization.

Discussion.—In practice, coherent phonons that can be optically driven can be manipulated from, for example, the pump fluence [66,67]. However, the coherent mode dominating the K-to-Q scattering has a large momentum, thus making the proposal of optical manipulation less straightforward. Nevertheless, these zone boundary phonons could be generated via the anharmonic coupling to the photo-excited coherent phonons, with the mechanism commonly known as nonlinear phononics [43,68–70]. Figure 4(b) schematically shows the down-conversion decay channel of the optically accessible A_1 mode [inset of Fig. 4(b)] into a pair of the target LA(M) modes.

To capture the phonon down-conversion, we carry out TDDFT-MD simulations by initially launching the A_1 mode with a large amplitude of 2.2 Å$\sqrt{\text{amu}}$ to mimic a resonant excitation via a strong THz laser. According to our numerical simulations, the peak field needed can be technically realized, and further reduced to a more practical value by delicate design of optical cavities [44–46,71] (Secs. S2, S10, and S11 of the Supplemental Material [40]). As is shown in Fig. 4(c), the A_1 mode oscillates coherently with an almost constant amplitude within our simulation timescale of 1 ps (Sec. S10 of the Supplemental Material [40]). However, the amplitude of the LA(M) mode grows exponentially, in analogy to the parametric resonance process [43,72]. Moreover, it becomes much larger than other modes in a longer timescale of ~3 ps, maintaining a good selectivity [Fig. S9(c) in the Supplemental Material [40]]. Based on an analytical model for nonlinear phononics (Sec. S11 in the Supplemental Material [40]), we find the LA(M) amplitude can be largely modified by the anharmonic coupling constant along with the A_1 mode amplitude. While the coupling constant is intrinsic to a material and approaches such as doping [73], strain [74,75] or structural engineering [47] might be needed to control their properties, the amplitude of A_1 mode has been shown to strongly depend on the pump laser frequency or fluence, thus could be more easily modulated [Fig. S8(a) in the Supplemental Material [40]] [76,77]. Therefore, through the tunability of the A_1 mode, we propose that the coherent LA(M) mode can be generated with varying amplitude, and our presented intervalley scattering mechanism could potentially be realized with a delicate design and proper driving conditions [78] (Secs. S11 and S12 of the Supplemental Material [40]).

Finally, as mentioned before, we find a trend of the electrons being scattered back to the K valley on a longer timescale (~700 fs); see Fig. S4 in the Supplemental Material [40]. This result is somewhat surprising since for thermal phonons one would expect a steady-state population from Fermi's golden rule [11,79]. Instead, such a reversible scattering process resembles the "Rabi oscillation," but induced by nonequilibrium coherent phonons. This may lead to innovative applications in lasing, "dark-to-bright" exciton switching, as well as valleytronics, where the valley degree of freedom concerns encoding, storing, and processing information.

Conclusions.—We perform a time-resolved calculation of the K-to-Q intervalley scattering in monolayer WSe$_2$ to address ultrafast electron dynamics via nonadiabatic coupling with coherent phonons. The time evolution of band energy and occupation number of K and Q valleys reveal a strong correlation between electron and lattice dynamics, which is further characterized and captured by our two-level model Hamiltonian. Based on the thorough understanding of the scattering dynamics, we propose that this process can be efficiently modulated by varying phonon amplitudes. Additionally, we suggest the anharmonic decay of zone-centered long-wavelength phonon as a possible channel to generate coherent oscillation of the short-wavelength modes that couple to the electronic system for future experimental realization of the observed scattering dynamics. We also note the Rabi oscillation between the K and Q valley occupation may provide an extra degree of freedom for further manipulation. Our work not only reveals the fundamental many-particle process out of thermal equilibrium, but also provides inspiration for the dynamical control of valleytronic devices.

---

[*]These authors contributed equally to this work.

[†]yaxianw@iphy.ac.cn

[‡]smeng@iphy.ac.cn

[1] A. Eftekhari, J. Mater. Chem. A **5**, 18299 (2017).

[2] V. K. Sangwan and M. C. Hersam, Annu. Rev. Phys. Chem. **69**, 299 (2018).

[3] J. R. Schaibley, H. Yu, G. Clark, P. Rivera, J. S. Ross, K. L. Seyler, W. Yao, and X. Xu, Nat. Rev. Mater. **1**, 16055 (2016).

[4] G. Wang, A. Chernikov, M. M. Glazov, T. F. Heinz, X. Marie, T. Amand, and B. Urbaszek, Rev. Mod. Phys. **90**, 021001 (2018).

[5] X. Xu, W. Yao, D. Xiao, and T. F. Heinz, Nat. Phys. **10**, 343 (2014).

[6] H. Li, J.-K. Huang, Y. Shi, and L.-J. Li, Adv. Mater. Interfaces **6**, 1900220 (2019).

[7] D. Christiansen, M. Selig, E. Malic, R. Ernstorfer, and A. Knorr, Phys. Rev. B **100**, 205401 (2019).

[8] Z. Jin, X. Li, J. T. Mullen, and K. W. Kim, Phys. Rev. B **90**, 045422 (2014).

[9] T. Sohier, D. Campi, N. Marzari, and M. Gibertini, Phys. Rev. Mater. **2**, 114010 (2018).

[10] M. Selig, G. Berghäuser, A. Raja, P. Nagler, C. Schüller, T. F. Heinz, T. Korn, A. Chernikov, E. Malic, and A. Knorr, Nat. Commun. **7,** 13279 (2016).

[11] M. Selig, G. Berghäuser, M. Richter, R. Bratschitsch, A. Knorr, and E. Malic, 2D Mater. **5,** 035017 (2018).

[12] J. Madéo, M. K. L. Man, C. Sahoo, M. Campbell, V. Pareek, E. L. Wong, A. Al-Mahboob, N. S. Chan, A. Karmakar, B. M. K. Mariserla, X. Li, T. F. Heinz, T. Cao, and K. M. Dani, Science **370,** 1199 (2020).

[13] S. Dong, M. Puppin, T. Pincelli, S. Beaulieu, D. Christiansen, H. Hübener, C. W. Nicholson, R. P. Xian, M. Dendzik, Y. Deng *et al.*, Nat. Sci. **1,** e10010 (2021).

[14] P. Hein, A. Stange, K. Hanff, L. X. Yang, G. Rohde, K. Rossnagel, and M. Bauer, Phys. Rev. B **94,** 205406 (2016).

[15] R.-Y. Liu, Y. Ogawa, P. Chen, K. Ozawa, T. Suzuki, M. Okada, T. Someya, Y. Ishida, K. Okazaki, S. Shin, T.-C. Chiang, and I. Matsuda, Sci. Rep. **7,** 15981 (2017).

[16] H. Hübener, U. De Giovannini, and A. Rubio, Nano Lett. **18,** 1535 (2018).

[17] M. Forst, R. Mankowsky, and A. Cavalleri, Acc. Chem. Res. **48,** 380 (2015).

[18] M.-X. Guan, X.-B. Liu, D.-Q. Chen, X.-Y. Li, Y.-P. Qi, Q. Yang, P.-W. You, and S. Meng, Phys. Rev. Lett. **128,** 015702 (2022).

[19] S. Ji, O. Granas, and J. Weissenrieder, ACS Nano **15,** 8826 (2021).

[20] P. G. Radaelli, Phys. Rev. B **97,** 085145 (2018).

[21] M. Y. Zhang, Z. X. Wang, Y. N. Li, L. Y. Shi, D. Wu, T. Lin, S. J. Zhang, Y. Q. Liu, Q. M. Liu, J. Wang, T. Dong, and N. L. Wang, Phys. Rev. X **9,** 021036 (2019).

[22] E. J. Sie, C. M. Nyby, C. Pemmaraju, S. J. Park, X. Shen, J. Yang, M. C. Hoffmann, B. Ofori-Okai, R. Li, A. H. Reid *et al.*, Nature (London) **565,** 61 (2019).

[23] C. Vaswani, L.-L. Wang, D. H. Mudiyanselage, Q. Li, P. M. Lozano, G. D. Gu, D. Cheng, B. Song, L. Luo, R. H. J. Kim, C. Huang, Z. Liu, M. Mootz, I. E. Perakis, Y. Yao, K. M. Ho, and J. Wang, Phys. Rev. X **10,** 021013 (2020).

[24] J. Zhou, H. Xu, Y. Shi, and J. Li, Adv. Sci. **8,** 2003832 (2021).

[25] C. P. Weber, M. G. Masten, T. C. Ogloza, B. S. Berggren, M. K. L. Man, K. M. Dani, J. Liu, Z. Mao, D. D. Klug, A. A. Adeleke, and Y. Yao, Phys. Rev. B **98,** 155115 (2018).

[26] M. Mitrano, A. Cantaluppi, D. Nicoletti, S. Kaiser, A. Perucchi, S. Lupi, P. Di Pietro, D. Pontiroli, M. Riccò, S. R. Clark *et al.*, Nature (London) **530,** 461 (2016).

[27] D. Fausti, R. Tobey, N. Dean, S. Kaiser, A. Dienst, M. C. Hoffmann, S. Pyon, T. Takayama, H. Takagi, and A. Cavalleri, Science **331,** 189 (2011).

[28] N. Punpongjareorn, X. He, Z. Tang, A. M. Guloy, and D.-S. Yang, Appl. Phys. Lett. **111,** 081903 (2017).

[29] D. Shin, S. A. Sato, H. Hübener, U. De Giovannini, N. Park, and A. Rubio, npj Comput. Mater. **6,** 182 (2020).

[30] A. S. Disa, T. F. Nova, and A. Cavalleri, Nat. Phys. **17,** 1087 (2021).

[31] S.-L. Yang, J. A. Sobota, Y. He, D. Leuenberger, H. Soifer, H. Eisaki, P. S. Kirchmann, and Z.-X. Shen, Phys. Rev. Lett. **122,** 176403 (2019).

[32] Z. Lin, Y. Liu, Z. Wang, S. Xu, S. Chen, W. Duan, and B. Monserrat, Phys. Rev. Lett. **129,** 027401 (2022).

[33] P. Hein, S. Jauernik, H. Erk, L. Yang, Y. Qi, Y. Sun, C. Felser, and M. Bauer, Nat. Commun. **11,** 2613 (2020).

[34] M. X. Na, A. K. Mills, F. Boschini, M. Michiardi, B. Nosarzewski, R. P. Day, E. Razzoli, A. Sheyerman, M. Schneider, G. Levy, S. Zhdanovich, T. P. Devereaux, A. F. Kemper, D. J. Jones, and A. Damascelli, Science **366,** 1231 (2019).

[35] S. Sakamoto, N. Gauthier, P. S. Kirchmann, J. A. Sobota, and Z.-X. Shen, Phys. Rev. B **105,** L161107 (2022).

[36] E. Runge and E. K. U. Gross, Phys. Rev. Lett. **52,** 997 (1984).

[37] S. Meng and E. Kaxiras, J. Chem. Phys. **129,** 054110 (2008).

[38] C. Lian, M. Guan, S. Hu, J. Zhang, and S. Meng, Adv. Theor. Simul. **1,** 1800055 (2018).

[39] C. Lian, S.-J. Zhang, S.-Q. Hu, M.-X. Guan, and S. Meng, Nat. Commun. **11,** 43 (2020).

[40] See Supplemental Material at http://link.aps.org/supplemental/10.1103/PhysRevLett.131.066401 for a description of our theoretical framework, detailed discussions on the excitonic effect, the deformation potential and nonadiabatic coupling matrix element, and nonlinear phononics, etc., which includes Refs. [41–57].

[41] M. Lazzeri, C. Attaccalite, L. Wirtz, and F. Mauri, Phys. Rev. B **78,** 081406(R) (2008).

[42] R. MacKenzie, E. Marcotte, and H. Paquette, Phys. Rev. A **73,** 042104 (2006).

[43] S. W. Teitelbaum, T. Henighan, Y. Huang, H. Liu, M. P. Jiang, D. Zhu, M. Chollet, T. Sato, É. D. Murray, S. Fahy *et al.*, Phys. Rev. Lett. **121,** 125901 (2018).

[44] D. M. Juraschek, Q. N. Meier, and P. Narang, Phys. Rev. Lett. **124,** 117401 (2020).

[45] D. M. Juraschek, T. Neuman, J. Flick, and P. Narang, Phys. Rev. Res. **3,** L032046 (2021).

[46] J. B. Curtis, M. H. Michael, and E. Demler, arXiv:2301.01884.

[47] T. Y. Jeong, B. M. Jin, S. H. Rhim, L. Debbichi, J. Park, Y. D. Jang, H. R. Lee, D.-H. Chae, D. Lee, Y.-H. Kim, S. Jung, and K. J. Yee, ACS Nano **10,** 5560 (2016).

[48] J. C. Tully, Faraday Discuss. **110,** 407 (1998).

[49] H.-Y. Chen, D. Sangalli, and M. Bernardi, Phys. Rev. Res. **4,** 043203 (2022).

[50] G. Onida, L. Reining, and A. Rubio, Rev. Mod. Phys. **74,** 601 (2002).

[51] J. Sun, C.-W. Lee, A. Kononov, A. Schleife, and C. A. Ullrich, Phys. Rev. Lett. **127,** 077401 (2021).

[52] K.-Q. Lin, C. S. Ong, S. Bange, P. E. Faria Junior, B. Peng, J. D. Ziegler, J. Zipfel, C. Bäuml, N. Paradiso, K. Watanabe, T. Taniguchi, C. Strunk, B. Monserrat, J. Fabian, A. Chernikov, D. Y. Qiu, S. G. Louie, and J. M. Lupton, Nat. Commun. **12,** 5500 (2021).

[53] M. Hellgren, J. Baima, R. Bianco, M. Calandra, F. Mauri, and L. Wirtz, Phys. Rev. Lett. **119,** 176401 (2017).

[54] J. A. Fülöp, S. Tzortzakis, and T. Kampfrath, Adv. Opt. Mater. **8,** 1900681 (2020).

[55] A. D. Koulouklidis, C. Gollner, V. Shumakova, V. Y. Fedorov, A. Pugžlys, A. Baltuška, and S. Tzortzakis, Nat. Commun. **11,** 292 (2020).

[56] X. Tong and M. Bernardi, Phys. Rev. Res. **3,** 023072 (2021).

[57] H. Padmanabhan, M. Poore, P. K. Kim, N. Z. Koocher, V. A. Stoica, D. Puggioni, H. (Hugo) Wang, X. Shen, A. H. Reid, M. Gu, M. Wetherington, S. H. Lee, R. D. Schaller, Z. Mao, A. M. Lindenberg, X. Wang, J. M. Rondinelli, R. D. Averitt, and V. Gopalan, Nat. Commun. **13,** 1929 (2022).

[58] U. Ritzmann, P. M. Oppeneer, and P. Maldonado, Phys. Rev. B **102,** 214305 (2020).

[59] X. Jiang, Q. Zheng, Z. Lan, W. A. Saidi, X. Ren, and J. Zhao, Sci. Adv. **7,** eabf3759 (2021).

[60] X.-B. Liu, S.-Q. Hu, D. Chen, M. Guan, Q. Chen, and S. Meng, Nano Lett. **22,** 4800 (2022).

[61] D. M. Kennes, E. Y. Wilner, D. R. Reichman, and A. J. Millis, Nat. Phys. **13,** 479 (2017).

[62] W. Miao and M. Wang, Phys. Rev. B **103,** 125412 (2021).

[63] M. Hellgren, J. Baima, R. Bianco, M. Calandra, F. Mauri, and L. Wirtz, Phys. Rev. Lett. **119,** 176401 (2017).

[64] S. Priyadarshi, I. Gonzalez-Vallejo, C. Hauf, K. Reimann, M. Woerner, and T. Elsaesser, Phys. Rev. Lett. **128,** 136402 (2022).

[65] W. Zhao, Z. Qin, C. Zhang, G. Wang, X. Dai, and M. Xiao, Appl. Phys. Lett. **115,** 243101 (2019).

[66] Y. Shinohara, K. Yabana, Y. Kawashita, J.-I. Iwata, T. Otobe, and G. F. Bertsch, Phys. Rev. B **82,** 155110 (2010).

[67] K. Uchida, K. Nagai, N. Yoshikawa, and K. Tanaka, Phys. Rev. B **101,** 094301 (2020).

[68] A. Subedi, C.R. Phys. **22,** 161 (2021).

[69] R. Mankowsky, M. Först, and A. Cavalleri, Rep. Prog. Phys. **79,** 064503 (2016).

[70] J. Z. Kaaret, G. Khalsa, and N. A. Benedek, J. Phys. Condens. Matter **34,** 035402 (2021).

[71] D. M. Juraschek and S. F. Maehrlein, Phys. Rev. B **97,** 174302 (2018).

[72] X. Hu and F. Nori, Phys. Rev. Lett. **76,** 2294 (1996).

[73] Y. Zhao, L. Du, W. Yang, C. Shen, J. Tang, X. Li, Y. Chu, J. Tian, K. Watanabe, T. Taniguchi, R. Yang, D. Shi, Z. Sun, and G. Zhang, Phys. Rev. B **102,** 165415 (2020).

[74] A. Subedi, Phys. Rev. B **95,** 134113 (2017).

[75] C. R. Zhu, G. Wang, B. L. Liu, X. Marie, X. F. Qiao, X. Zhang, X. X. Wu, H. Fan, P. H. Tan, T. Amand, and B. Urbaszek, Phys. Rev. B **88,** 121301(R) (2013).

[76] M. Först, C. Manzoni, S. Kaiser, Y. Tomioka, Y. Tokura, R. Merlin, and A. Cavalleri, Nat. Phys. **7,** 854 (2011).

[77] R. Mankowsky, A. von Hoegen, M. Först, and A. Cavalleri, Phys. Rev. Lett. **118,** 197601 (2017).

[78] F. Bussolotti, J. Yang, H. Kawai, J. Y. Chee, and Kuan Eng Johnson Goh, Phys. Rev. B **103,** 045412 (2021).

[79] D. W. Snoke, *Solid State Physics: Essential Concepts,* 2nd ed. (Cambridge University Press, Cambridge, England, 2020).